# Molecular modeling of proteinlike inclusions in lipid bilayers: Lipid-mediated interactions

Richard A. Kik, Frans A. M. Leermakers, and J. Mieke Kleijn*

*Laboratory of Physical Chemistry and Colloid Science, Wageningen University, P.O. Box 8038, 6700 EK Wageningen, The Netherlands*

(Received 26 August 2009; revised manuscript received 11 November 2009; published 18 February 2010)

We investigated the insertion of transmembrane structures in a lipid bilayer and their interactions using self-consistent field theory. The lipids are coarse-grained on a united-atom level and consist of a phosphatidylcholinelike headgroup and two hydrophobic tails. The inclusions, acting as simple models for proteins that span biological membranes, are rigid rods (radius $R$) with a hydrophobic surface and hydrophilic end caps. The insertion free energy $\Omega$ of an individual rod is strongly regulated by the affinity between its hydrophobic surface and the lipid tails. This affinity also controls the best match of the hydrophobic length of the rod with that of the bilayer. The line tension $\tau(=\Omega/2\pi R)$ is practically independent of $R$. The perturbations in the bilayer as a function of distance from the inclusion, have the shape of a damped oscillation. The wavelength and decay length are related to the elastic properties of the bilayer and do not depend on $R$. These results are used to analyze how the lipid matrix affects the interaction between transmembrane objects, for computational reasons considering the limit of $R\rightarrow\infty$. Contributions on different length scales can be distinguished: (i) a long-range elastic interaction, which is an exponentially decaying oscillation; (ii) an exponentially decaying repulsion on an intermediate length scale, resulting from the loss of conformational entropy of the lipid tails; and (iii) a short-range interaction due to the finite compressibility of the lipid tails, which manifests either as a depletion attraction if there is no affinity between the tails and the inclusions' surface or, otherwise, as an oscillatory structural force.

DOI: 10.1103/PhysRevE.81.021915 PACS number(s): 87.10.Hk, 87.16.aj, 87.16.dt

## I. INTRODUCTION

The organization of transmembrane structures, such as peptides and proteins, in a biological membrane is determined by many factors. A well studied and important aspect, which we addressed in an earlier paper [1], is the hydrophobic mismatch, i.e., the difference between the length of the hydrophobic part of the transmembrane structure and the thickness of the hydrophobic part of the unperturbed bilayer. When there is such a mismatch, the bilayer will adapt its structure to avoid contact between hydrophobic parts and water. The mismatch issue is of key importance for the functioning and activity of various integral membrane-bound proteins and peptides, as has been shown in several experimental studies [2–11]. Hydrophobic mismatch and the insertion energy have been explored thermodynamically and experimentally in particular for alpha helices, using the translocon channel of the endoplasmic reticulum where most membrane proteins get inserted into lipid membranes, thereby providing the hydrophobicity scale for amino acids [12,13]. In addition, a significant theoretical effort has already been undertaken to gain insight into the physical aspects of the embedding of proteins and peptides in lipid bilayers. A review in this area is given by Sperotto *et al.* [14]. In some of the studies involved, the elasticity theory developed by Helfrich [15] has been extended to get phenomenological insight into the energetic and structural consequences of the hydrophobic mismatch [16–21]. An important addition to this elasticity theory was the chain directors model, which accounts for the conformational restrictions of the lipid chains in the vicinity of the inclusion that determine local deformations of the bilayer [22]. In other studies [23,24], including our own, detailed statistical mechanical models are used. In these models molecular interaction forces and the hydrocarbon chain conformations are taken into account. The model that we use and that of, e.g., Fattal and Ben-Shaul [25] have much in common. However, our approach is somewhat more advanced as we impose no *a priori* positional constraints on the individual lipids.

In our previous paper [1] we described the structural perturbations of inserting a rigid inclusion in a tensionless bilayer. It was found that the free energy of insertion is at a minimum at a small negative hydrophobic mismatch, i.e., when the hydrophobic thickness of the inclusion is somewhat smaller than that of the bilayer. The bilayer perturbations have an oscillating character and decay exponentially with distance to the inclusion. The wavelength of the oscillations as well as the decay length that we found are the same as follow from elasticity theory.

In this paper we will first address the effect of the radius of a rigid cylindrical object on the bilayer perturbation and the free energy of insertion. This is highly interesting from a biological point of view, since transmembrane peptides and proteins vary substantially in size (from about 0.5 to 5 nm). For example, the radius of beta barrels, i.e., beta sheets that form closed, rigid structures in membranes (commonly found in porins and other proteins that span cell membranes), varies depending on the number of $\beta$-strands in the structure [26]. The effect of the size of a transmembrane object on the lipid bilayer structure has been studied before [27–29]. Schmidt *et al.* [30] report on a dissipative particle dynamics study wherein they show that proteins can aggregate in the bilayer due to a hydrophobic mismatch. Lagüe *et al.* [28,29] investigated the influence of the radius of rigid cylinders, using molecular dynamics in combination with statistical mechanical integral equation theory. Around these rigid ob-

*Corresponding author.

 

jects on different length scales distinct bilayer perturbations were found. Their complex results call for complementary approaches directed to unravel this, not in the least because such bilayer perturbations are important for interactions between transmembrane structures. Our self-consistent field (SCF) method is suitable to do such a job, especially for the properties on the nanometer length scale and above. In addition, we will consider the effect of nearest-neighbor interactions (the chemical affinity) between the lipid tail segments and the inclusion and show that these largely determine the free energy of insertion. Until now not much is known about the role of such interactions, since in most theoretical studies it has been assumed that the lipids freely adjust their conformation to overcome any "interaction" mismatch and possible nearest-neighbor interactions have been tacitly left out the analysis.

Another important motive to first determine the effect of the radius of the inclusion on the lipid bilayer is related to the main subject of this paper, that is on how the lipid bilayer mediates the interaction between transmembrane objects. Due to computational reasons we focus on the interaction between two flat walls, mimicking large inclusions. By ignoring the curvature of inclusions, we can make use of the symmetry and cast the problem in a two-gradient SCF analysis.

In the past a number of studies has been performed to get insight into the phenomenon of lipid-mediated interactions in bilayer membranes [22,28,29,31–40]. In most of these studies the elasticity theory was used [33,34,37–39], but also a molecular field theory was applied [22,31], as well as the phenomenological Landau theory [32], and some Monte Carlo [36] and molecular dynamics simulations [28,29]. In all of these studies however there was no effective adsorption of the lipid tails to the inclusion's surface. As mentioned above, we will also consider the nearest-neighbor interactions between the tail segments and the inclusions, and we will show that these play an important role in the interaction between two transmembrane objects. Our method is computationally inexpensive and numerically very accurate so we can obtain systematic predictions for the complex problem of lipid-mediated interactions.

## II. THEORY AND METHODS

Molecular modeling of densely packed molecular assemblies such as lipid bilayers is an active branch of science. Ideally one would like to compute for a given model (the architecture of the molecules and the set of interactions) the exact partition function. However, for such complicated systems these are not available. In such a situation one can choose between two distinctly different approaches. A first route is to use the molecular model in an appropriate simulation, e.g., Monte Carlo or molecular dynamics. Even though one will not estimate the partition function in this approach (and hence can not easily compute the entropy, free energies etc.), structural information is accurately obtained by averaging along a simulation trajectory. Here we are interested not only in structural but also in thermodynamic information and thus we do not choose to follow the simulation route. A second route, applied in this paper, is to make use of so-called mean field approximations and compute a mean-field free energy. We do this by following the self-consistent field formalism. The current SCF model has been successfully used to study self-assembling structures, such as bilayers, micelles and vesicles [1,41–43].

In this model the molecules present in the system are coarse-grained on the united atom level, i.e., they consist of segments, which are the basic building blocks. Excluded-volume interactions between pairs of segments are replaced by the interaction of a single segment with an external potential field, which is the basic approximation in mean-field theory. This potential field $u_{\mathrm{A}}(\mathbf{r})$ contains all the potential energy contributions to bring a segment A from the bulk solution to position $\mathbf{r}$.

To facilitate the numerical evaluation the $3d$ space is represented by a lattice; segments of molecules are restricted to sit on lattice sites. All segments have the same volume as a lattice site. Such a lattice allows us to accurately and efficiently account for the different conformations of chainlike and branched molecules.

Obviously, the potential field experienced by each segment is determined by the segment density profiles, i.e., the spatial distributions of all types of segments over the system, and vice versa. The target of SCF modeling is to find the optimal self-consistent combination of segment density profiles and potential fields. This is done by optimizing the Helmholtz energy $F$ of the system, which is a functional of all potentials $u_{\mathrm{A}}$ and volume fractions $\varphi_{\mathrm{A}}$,

$$F[u,\varphi] = k_{\mathrm{B}}T\sum_{\mathrm{i}} n_i \ln\frac{C_i}{Q_i[u]} - \sum_{\mathbf{r}}\sum_{A} u_A(\mathbf{r})\varphi_A(\mathbf{r}) + F^{\mathrm{int}}[\varphi]. \tag{1}$$

In this expression the first two terms represent the entropic contribution, in which $Q_{\mathrm{i}}$ is the single (chainlike) molecule partition function and $C_{\mathrm{i}}$ a normalization constant [44]. The third term stands for the enthalpic contribution.

The Helmholtz energy is coupled to the partition function $Q(n,V,T)$ through $F=k_{\mathrm{B}}T\ln Q(n,V,T)$, where $n,V,T$ stands for fixed total numbers of molecules of each type $n_{\mathrm{i}}$, a given volume of the system and a given temperature, respectively; $k_{\mathrm{B}}$ is the Boltzmann constant. Thus, optimizing $F$ with respect to $u_{\mathrm{A}}$ and $\varphi_{\mathrm{A}}$ for all coordinates and segment types, with the boundary condition that $\Sigma_{\mathrm{A}}\varphi_{\mathrm{A}}(\mathbf{r})=1$, gives

$$\frac{\partial F}{\partial u_{\mathrm{A}}(\mathbf{r})} = -\sum_{\mathrm{i}} \frac{n_i k_{\mathrm{B}}T\,\partial\,\ln Q_i}{\partial u_{\mathrm{A}}(\mathbf{r})} - \varphi_{\mathrm{A}}(\mathbf{r}) = 0, \tag{2}$$

$$\frac{\partial F}{\partial \varphi_{\mathrm{A}}(\mathbf{r})} = -u_{\mathrm{A}}(\mathbf{r}) + \frac{\partial F^{\mathrm{int}}}{\partial \varphi_{\mathrm{A}}(\mathbf{r})} = 0. \tag{3}$$

This set of equations, which is the basis of any self-consistent field theory, specifies how to calculate the segment density profiles from the segment profiles and vice versa. A numerical algorithm is used to find the corresponding system, better known as the self-consistent field solution. From analysis of the density profiles the structural properties of the system can be found, while the thermodynamic properties

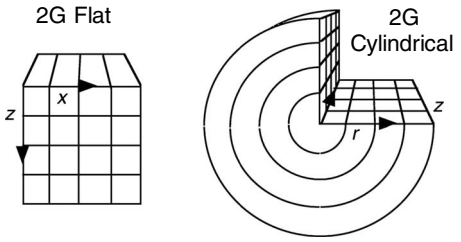


FIG. 1. The two lattice geometries applied in this paper. In both coordinate systems two gradients in densities and potentials can be accounted for. The arrows point in the directions of these gradients. We use $\mathbf{r}=(x,z)$ in the flat and $\mathbf{r}=(r,z)$ in the cylindrical case.

follow directly from differentiation of the Helmholtz energy [45].

Details on the modeling of lipid bilayers and the effect of rigid transmembrane inclusions can be found in our previous paper [1]. Here we give only the key characteristics. In this particular study two-gradient (2G) flat and cylindrical coordinate systems as shown in Figure 1 are used that allow us to study the laterally inhomogeneous lipid bilayers. The two gradients in the molecular structure are perpendicular to the surface of the bilayer and perpendicular to the surface of the inclusion (in the plane of the bilayer). For the investigation of the effect of the radius $R$ of the inclusion on the free energy of insertion and on the lipid bilayer structure we make use of the 2G cylindrical coordinate system. Unless the focus is on confinement issues, the system size is chosen large enough so that at its boundaries in the radial, $r$, direction the effect of the inclusion has vanished and in the $z$ direction the bulk solution has become homogeneous. The lipid-mediated interactions between two inclusions have been calculated on the 2G flat lattice.

As told, the SCF method includes a mean-field simplification. This means that the actual position of segments in the $y$ direction for 2G flat and for the sites in a given shell in 2G cylindrical are averaged over, while keeping track of the fraction of sites occupied for each segment type $\varphi_A(z,x)$ or $\varphi_A(z,r)$ for the flat and cylindrical cases, respectively. At the same time interactions between pairs of segments are replaced by the interaction of a single segment with a potential field $u_A(\mathbf{r})$, with $\mathbf{r}=(z,x)$ in 2G flat and $\mathbf{r}=(z,r)$ in 2G cylindrical geometry. As it follows from optimizing the free energy with respect to the segment distributions, the potential field is a function of the volume fractions [cf. Eq. (3)],

$$u_A(\mathbf{r}) = u'(\mathbf{r}) + k_B T \sum_B \chi_{AB}[\langle \varphi_B(\mathbf{r})\rangle - \varphi_B^b] \qquad (4)$$

where $u'(\mathbf{r})$ is the excluded-volume potential which arises from the incompressibility constraint $\Sigma_A \varphi_A(\mathbf{r})=1$. In other words, it is the energy needed to generate a vacant site at position $\mathbf{r}$ to insert segment A. The second term accounts for the nonideal interactions of segment A with all other segment types, denoted by B. The Flory-Huggins nearest-neighbor exchange energy parameter is denoted by $\chi_{AB}$. It accounts for the interaction between segment A and segment B and is negative when the AA and BB interactions are energetically unfavorable compared to the AB interactions and positive when it is the other way around (resulting in an effective attraction or repulsion between A and B, respectively). The parameter $\varphi_B$ is the volume fraction of B and the superscript b refers to the bulk solution, i.e., the aqueous solution at large distance from the bilayer. The angular brackets represent a local average. Equation (7) is used to compute the potentials from the volume fractions.

As explained above, the SCF machinery also needs the inverse, i.e., we have to compute the volume fractions from optimizing the free energy with respect to the segment potentials. It will be clear that this problem is in general much more involved as it needs information of all possible spatial configurations of the molecules. For very short molecules, it is feasible to generate all possible conformations of the molecules on the lattice (this may be referred to as the set of self-avoiding walk SAW conformations). In such a case the procedure simply proceeds to enumerate for each conformation $c$ the potentials felt by its segments which we may collect in $u_c$. The Boltzmann weight gives the statistical weight of this conformation, i.e., $G_c \propto \sim \exp(-u_c/k_B T)$. Knowing the positions of all the segments and the statistical weights, it is then straightforward to recover all the distributions $\varphi_A(\mathbf{r})$. However, the procedure sketched for the SAW case is, for molecules with more than ten segments, computationally too expensive. Here we use a more approximate chain model, namely the freely jointed chain (FJC). In FJC two consecutive segments in the chain occupy neighboring sites on the lattice, but segments further along the chain are allowed to visit the same coordinate (remember there are multiple sites at each coordinate). The excluded-volume problem is "repaired" somewhat by requiring that on average each site is visited just once (incompressibility constraint). Within this chain model there exists a propagator formalism to compute the volume fractions efficiently. As this propagator formalism is somewhat involved for branched molecules and because it has been presented many times before in the literature (see, e.g., Refs. [45,46]) we do not give more details here.

Below we will typically focus on the thermodynamic response when a proteinlike inclusion is inserted in a tensionless bilayer or when two inclusions are brought in close proximity. In such a system the chemical potential of the lipids as well as that of water is fixed (otherwise the membrane tension would change) and hence the grand potential $\Omega$ is our characteristic function for this open system [47]. The grand potential is found by subtracting all chemical potential contributions from the free energy, i.e., $\Omega=F-\Sigma_i \mu_i n_i$. Note that in this quantity the proteinlike inclusion is treated as a local boundary condition, which effectively means that its internal free energy characteristics are irrelevant for the problem at hand.

It is well known [48,49] that $\Omega=\Sigma_{\mathbf{r}}\omega(\mathbf{r})L(r)$, where $L(r)$ is the number of sites in the radial coordinate (in the cylindrical coordinate system) and $\omega(\mathbf{r})$ is the grand potential density at coordinate $\mathbf{r}$. Due to nonlocal binary interactions, $\omega(\mathbf{r})$ is not uniquely defined. Below we make a reasonable choice to distribute the nonlocal interactions evenly over the sites that are involved. By doing so, it is possible to compute, e.g., the local membrane tension [$\gamma(x)$ in the 2G flat or $\gamma(r)$ in the 2G cylindrical coordinate system] by summing the grand po-

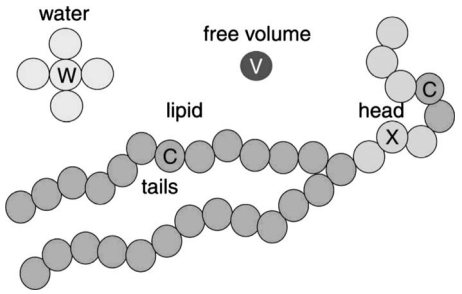


FIG. 2. The molecules that are used in the calculations are coarse-grained on a molecular level. The water molecules are represented by a cluster of five identical W-segments, while the free volume is a single hydrophobic V segment. The most complex molecule in the system is the lipid. It has two tails, each consisting of $t$ hydrophobic segments C (representing a $CH_2$- or a $CH_3$-group). The lipid head comprises two hydrophilic regions consisting of three segments X which are spaced by two hydrophobic segments that are identical to the tail segments.

tential density along the $z$ direction, i.e., $\gamma(x)=\Sigma_z\omega(z,x)$ and similarly for the cylindrical coordinate system. We will use these local tensions below [see Eq. (10)].

One of the primary quantities is the lipid (and water) contribution to the grand potential when a proteinlike inclusion is inserted. This insertion free energy is given by the difference between the grand potential with and that without the inclusion in the bilayer. As the membrane is free of tension, the reference grand potential is zero and thus we conclude that the grand potential $\Omega$ is interpreted as the free energy of insertion. It proves convenient to normalize this quantity by the contour length of the cylindrical inclusion to obtain $\tau=\Omega/2\pi R$, which may be called the line tension as it has the dimension $k_BT/\ell$ (with $\ell$ the size of a lattice site, corresponding to 0.2–0.3 nm [45]). In general the value of this line tension is a function of the curvature of the inclusion, $J_p=1/R$.

In the second part of this paper we turn our attention to the free energy of interaction between two (flat) inclusions. Again the proteinlike inclusions effectively are accounted for by the boundary condition and the free energy of interaction is found by the difference between the inclusion energy at distance $H$ computed to that at very large inclusion distances, i.e., $F(H)\equiv\Omega(\mathrm{H})-\Omega(\infty)$. In this geometry the grand potential is given per unit length of the inclusion (in the $y$ direction) and we focus on the free energy of interaction normalized to one proteinlike surface.

For the properties of the bilayer in the absence of inclusions we refer to our previous paper [1] and below we only briefly comment on the parameters used. All length parameters are given as dimensionless quantities (normalized to the size of a lattice site $\ell$). The molecular architecture of the molecules is presented in Fig. 2. The lipid molecules consist of two hydrophobic tails of length (number of segments) $t$ coupled to a hydrophilic headgroup. The headgroup mimics phosphatidylcholine, containing two hydrophilic fragments of three segments spaced by two hydrophobic segments.

The relevant Flory-Huggins interaction parameters are collected in Table I. In various studies we have worked towards the set of parameters needed to calculate the properties

TABLE I. The Flory-Huggins nearest-neighbor exchange parameters for the various pairs of segments. A positive value means that the net interaction is repulsive and a negative value represents a net attractive interaction (with respect to the interaction between identical segments).

| Segment | W | C | X | V | S | E |
|---|---|---|---|---|---|---|
| E | 0 | 2.0 | 0 | 2.3 | 0 | 0 |
| S | 2.0 | −1.0 | 2.0 | 1.5 | 0 | |
| V | 2.3 | 1.5 | 2.3 | 0 | | |
| X | −0.5 | 2.5 | 0 | | | |
| C | 1.1 | 0 | | | | |
| W | 0 | | | | | |

of the lipid bilayer (without inclusions). It has been well established that this set works very well for modeling lipid bilayer membranes [42,43,45], some of the parameters are based on experimental data, for example, the value for $\chi_{WC}$ is based on the tail length dependence of the critical micelle concentration of surfactants [50], while the value of 2.3 for $\chi_{WV}$ has been chosen in such a way that the calculated surface tension of the VW interface is of the same order of magnitude as experimentally determined values for the air/water interface. The values of the other interaction parameters are to some extent arbitrary, since they cannot be determined directly from experimental data. We emphasize that in the present paper the parameter set for the lipid bilayer is not the subject of study; the key parameters here are the radius of the inclusion, $R$, and its interaction with the lipid tails represented by $\chi_{SC}$.

The value of 1.1 for $\chi_{WC}$ implies that C and W effectively repel each other and this drives the self-assembly of the lipids. On the other hand, the lipid headgroup contains six hydrophilic (X) segments that contribute to the stopping force for self-assembly. The interaction between these segments and water is chosen to be slightly attractive ($\chi_{XW}=-0.5$), while demixing of the lipid tails and heads is established with $\chi_{XC}=2.5$.

From experiments it is known that water is almost completely absent in the hydrophobic core of lipid bilayers [51,52]. For this reason we have implemented water as a small compact cluster of five segments as shown in Figure 2. Such clusters of water will not easily partition in the core, and as a result in this model the water content in the bilayer core is less than 1 volume percent. Furthermore, we account for some volume fraction of vacant sites (V) in the system. The bulk fraction of free volume in the aqueous solution is $\varphi_V^b=0.051\,396$, which is fixed throughout all calculations.

The hydrophobic length of the inclusions, $D$, equals 8 and the two hydrophilic end caps have a length of 1. See Fig. 3. The parameters for the interactions of the end caps E with the lipid headgroup segments, $\chi_{EX}$, and with water, $\chi_{EW}$, have been set to zero for simplicity. We chose the interactions of the rigid hydrophobic surface S with water and with the hydrophilic headgroup segments to be unfavorable, i.e., $\chi_{SW}=\chi_{SX}=2$. The interaction of the rigid hydrophilic end caps with the hydrophobic lipid tails must be unfavorable and again for simplicity reasons the same value as the latter

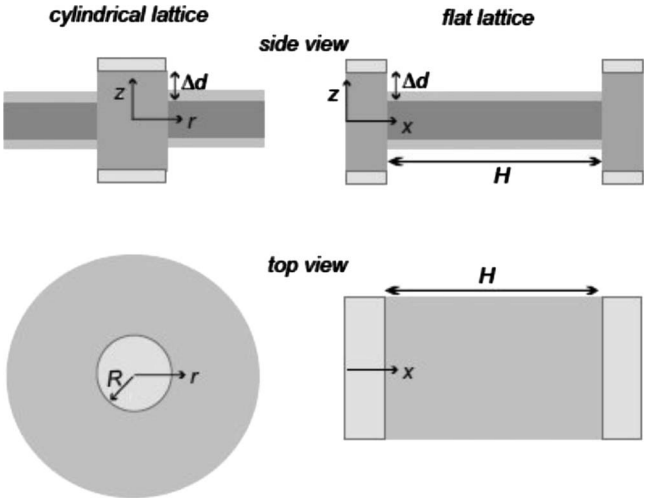


FIG. 3. Schematic representation of the insertion of inclusions (top: side views, bottom: top views). The cylindrical two-dimensional lattice (left) is used when a single inclusion is incorporated into the bilayer. When two inclusions are inserted in the bilayer a two-dimensional lattice (right) is needed. The distance $H$ between the hydrophobic surface of these inclusions can be varied. The hydrophobic mismatch $\Delta d$ is defined as $(D-d_l^0)/2$, with $D$ the hydrophobic length of the inclusion and $d_l^0$ the hydrophobic thickness of the unperturbed bilayer.

two was taken, i.e., $\chi_{EC}=2$. For the interaction with the vacancies $\chi_{EV}=\chi_{VW}=\chi_{VX}=2.3$, which implies that the V segments are strongly repelled by the polar segments. (Recall that the interaction between C and V is also repulsive, i.e., $\chi_{CV}=1.5$.) Unless stated otherwise the interaction between the hydrophobic surface of the inclusion and the hydrophobic tails is attractive, i.e., $\chi_{SC}=-1.0$. The interactions of the hydrophobic surface with the V units are in between the interactions with the hydrophilic and the hydrophobic segments, i.e., $\chi_{SV}=1.5$.

In Fig. 4 an example is given of a segment density profile across a bilayer composed of lipids with tail length $t=18$. It shows that water solvates the headgroup but not the tails, that the free volume V partitions more in the bilayer than in the aqueous solution, that the size of the bilayer headgroup region is comparable to the hydrophobic region and that the segment density in the core of the hydrophobic region is

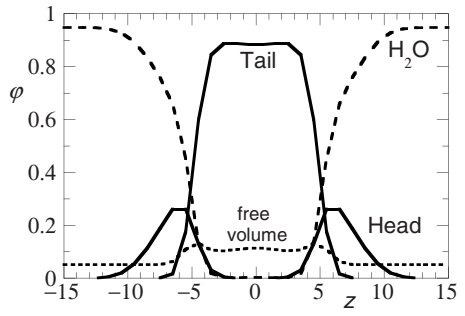


FIG. 4. Volume fraction profile across a tensionless planar lipid bilayer with tail length $t=18$. The volume fraction profiles of the tail and the head segments are depicted, as well as those of free volume and water.

homogeneous. From our previous results [1] we know that in this model the hydrophobic bilayer thickness $d_\ell^0$, the area per lipid molecule $a_0$, and the elasticity moduli of a tensionless bilayer all show a linear dependence on the lipid tail length $t$. For the unperturbed bilayer $d_l^0$ is obtained from the volume fraction profile of the C segments as the distance between the positions where the volume fraction equals 0.5. For $t=18$ the hydrophobic thickness $d_\ell^0$ amounts to 10.8 (corresponding to about 3 nm), while the area per molecule $a_0$ is 8.38 (0.6–0.7 nm$^2$). Many features in Fig. 4 are quantitatively in line with molecular dynamics (MD) results as has been shown a number of years ago [45].

The hydrophobic mismatch between the inclusion and the lipid bilayer is defined as $\Delta d=(D-d_l^0)/2$, which is schematically depicted in Fig. 3. For a given value of $D$, the hydrophobic mismatch is linear in $t$. For example, for $D=8$ (which is used throughout this paper): $\Delta d=2.57-0.218t$.

In our previous paper [1] we incorporated a cylindrical inclusion of radius $R=6$ in a lipid bilayer and varied its hydrophobic length $D$. The line tension was found to have a parabolic dependence on the hydrophobic mismatch between the inclusion and the bilayer,

$$\tau = W(\Delta d - \Delta d_{\min})^2 + \tau_{\min} \tag{5}$$

with $W$ the width of the parabola, $\tau_{\min}$ the minimum line tension and $\Delta d_{\min}$ the "optimal" hydrophobic mismatch, i.e., the mismatch of the lowest free energy. We showed that an increase in $D$ only affects $\tau_{\min}$ significantly, which can be attributed to the increased interaction area between the inclusion's hydrophobic surface and the bilayer.

## III. RESULTS AND DISCUSSION

### A. Interaction between the inclusion and the lipid tails

There are little data available on the role of the contact interaction between the hydrophobic part of transmembrane structures and the lipid tails. In theoretical modeling it is typically assumed that the lipids adjacent to an inclusion experience steric hindrance, while specific interactions are not considered. Because of steric hindrance the lipids around the inclusion lose part of their conformational entropy compared to the situation in the unperturbed bilayer. As a consequence the lipid tails will to some extent avoid the surface of the transmembrane structure. Calculations show that the tail segments compete with the V units for the sites on the hydrophobic part of the inclusion's surface. This means that if the tail segments deplete from the inclusion, the V units take their place.

In contrast to our model transmembrane objects, the surface of a real transmembrane structure like a peptide or protein is not smooth and rigid, but molecularly rough with several more or less mobile groups attached to it, which may have different affinities to the lipid tails. Therefore, we should account for the somewhat unrealistic conformational entropy loss suffered by the tails in our model and this can be done through the contact interaction between tail segments and surface of the rigid object. This issue is well known in polymer adsorption theory, where the concept of a critical

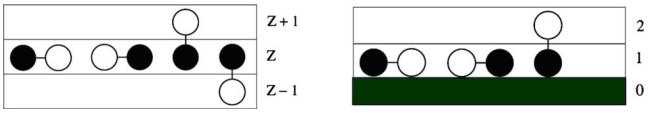


FIG. 5. (Color online) Schematic two-dimensional illustration of the entropy loss of dimers adjacent to a rigid surface. Having the position of the black segment of the dimer fixed, in bulk (left) the white segment can obtain four different positions, whereas adjacent to a rigid surface (right) it can only sit at three different positions. Thus, the bond between the two segments has lost conformational entropy when the dimer is near a surface.

adsorption energy is introduced, i.e., the enthalpy that exactly counterbalances the entropy loss near the surface [53,54]. To give an idea of the magnitude of this critical adsorption energy, in Fig. 5 all possible conformations of dimers in a two-dimensional system are shown, keeping the position of one segment fixed. In the bulk there are four possible positions for the other segment, whereas near the surface there are only three. Generally, the entropy loss for a bond between two segments near a surface, implying that one out of $Z$ directions is blocked by the surface, amounts to $\Delta S/k_B = -\ln(1-1/Z) \approx 1/Z \equiv \lambda_1$. As a segment C next to the inclusion has $\lambda_1$ contacts with S, the exchange with V gives an energy effect, $\Delta u/k_B T = \lambda_1(\chi_{SC} - \chi_{SV})$. This means that $\chi_{SC} - \chi_{SV}$ has to be approximately $-1$ in order to compensate for this entropic loss. When the enthalpic contribution is larger there will be an excess of C near the surface, and when it is lower C will deplete. However, this simple analysis does not account for the fact that in the lipid bilayer the tails are strongly aligned in the $z$ direction, parallel to the inclusion. We therefore have no accurate evaluation of the true critical adsorption energy. In particular we expect this also to depend on the hydrophobic mismatch.

In Fig. 6(a) the volume fraction profile of the lipid tails next to a rigid rod of radius $R=6$ and hydrophobic length $D=8$ has been plotted for three different values of the interaction parameter $\chi_{SC}$. The hydrophobic mismatch $\Delta d = -0.12$. The profile on the top where $\chi_{SC}=-2$ shows an increase in tail density adjacent to the inclusion, represented by the dark area. Furthermore, it can be seen that the bilayer

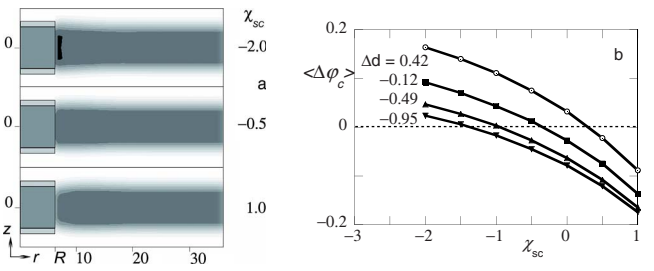


FIG. 6. (Color online) (a) Two-dimensional volume fraction profiles of the lipid tail segments near a rigid object (on the left side of each plot), for a hydrophobic mismatch $\Delta d = -0.12$ (tail length $t=12$) and different values for the interaction parameter $\chi_{SC}$. The lipid tail volume fraction increases from white to black. (b) The deviation of the average tail segment density at $r=R+1$ from that at $r \gg R$, $\langle \Delta\varphi_C \rangle$, as a function of $\chi_{SC}$ for various values of $\Delta d$ as indicated.

thickness $d_l$ in the first layers next to the inclusion is larger than for the unperturbed bilayer. These two features indicate that for this case the enthalpic contribution to the insertion free energy is larger than the conformational entropic loss. In the profile for $\chi_{SC}=-0.5$, the tail density $\varphi_C$ and bilayer thickness $d_l$ are approximately constant, suggesting that in this case the favorable interaction between the C segments and the inclusion counterbalances the entropic loss of the lipid tails. In the profile at the bottom, where $\chi_{SC}=1$, there is no attractive SC interaction to compensate for the entropic loss, resulting in a decrease in $d_l$ and $\varphi_C$ near the inclusion.

Since the effect of insertion of the object is reflected in a complicated way in both the thickness and the density of the bilayer, it is difficult to accurately determine the critical value of $\chi_{SC}$ and we need an operational definition. For this we have evaluated the ($z$-averaged) deviation in the tail segment density adjacent to the object (i.e., for $r=R+1$) from that in the undisturbed bilayer, given by

$$\langle \Delta\varphi_C \rangle = \frac{1}{D} \sum_{z=-D/2}^{z=D/2} [\varphi_C(R+1,z) - \varphi_C(r \gg R,z)] \qquad (6)$$

We now define the critical value $\chi_{SC}^{cr}$ as the value of $\chi_{SC}$ for which $\langle \Delta\varphi_C \rangle = 0$. In Fig. 6(b) we present $\langle \Delta\varphi_C \rangle$ as a function of $\chi_{SC}$ for several values of $\Delta d$. As expected $\langle \Delta\varphi_C \rangle$ decreases when $\chi_{SC}$ increases, i.e., with decreasing attractive interaction, and $\chi_{SC}^{cr}$ is a function of the hydrophobic mismatch $\Delta d$. Further analysis reveals that there is a linear relation between $\chi_{SC}^{cr}$ and $\Delta d$, for the chosen set of parameters given by $\chi_{SC}^{cr} = -0.23 + 1.24\Delta d$. Thus, for $\Delta d = 0$, $\chi_{SC}^{cr} - \chi_{SV}$ amounts to $-1.73$. This is significantly more negative than $-1$, the above mentioned critical adsorption value that is found for polymers adsorbing on a rigid wall. For a positive value of $\Delta d$, the bilayer thickness adjacent to the inclusion is larger than $d_l^0$, and therefore the average tail density is increased with respect to the unperturbed bilayer. This increase in tail density opposes the effect of entropic loss of the tails near the rigid wall and as a consequence $\chi_{SC}$ has to be less attractive to keep $\langle \Delta\varphi_C \rangle \approx 0$. In the case of a negative $\Delta d$ the situation is just the opposite, i.e., the bilayer thickness adjacent to the inclusion is decreased and this results in an extra depletion contribution (since the C segments also avoid contact with the hydrophilic end caps of the inclusion) on top of the conformational entropic loss.

Obviously, the interaction parameter $\chi_{SC}$ influences not only the bilayer structure but also the free energy of insertion of the inclusion into the bilayer. As mentioned already the SCF method allows to straightforwardly computing the free energy of insertion $\Omega$ and the line tension $\tau$. In Fig. 7(a) the strong dependence of the minimal line tension $\tau_{min}$ [defined in Eq. (8)] on $\chi_{SC}$ is shown, for $R=6$. To a good approximation $\tau_{min}$ is proportional to $\chi_{SC}$ and increases with $2.03k_BT$ per unit of $\chi_{SC}$. This means that the total insertion energy $\Omega = 2\pi R\tau$ increases with no less than $76.5k_BT$ when $\chi_{SC}$ is increased with one unit. From this we can understand that for integral membrane peptides and proteins in biological systems, accurate matching of the amino acid residues embedded in the hydrophobic core of the lipid bilayer with respect to their affinity to the lipid tails, is of crucial importance to

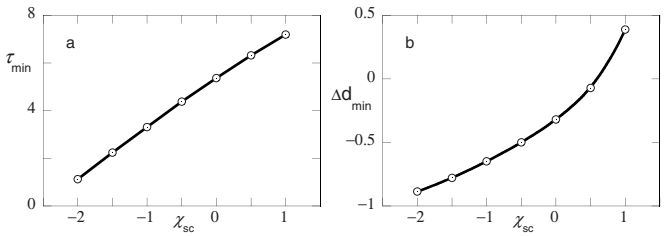


FIG. 7. The dependence of (a) the minimal line tension $\tau_{\min}$ and (b) the hydrophobic mismatch $\Delta d_{\min}$ at minimal line tension $\tau_{\min}$ on the Flory-Huggins interaction parameter $\chi_{SC}$ for the interaction between the hydrophobic part of the inclusion and the lipid tail segments.

avoid excessively large values of the insertion free energy. Indeed most of these residues should have a hydrophobic character and in line with experimental data [11–13,55] the number and position of polar residues largely determines whether a peptide or protein is inserted in the bilayer or not. It has been found that direct protein-lipid interactions are crucial during translocon-mediated membrane insertion [13,56].

The small deviation from the linear relation between $\tau_{\min}$ and $\chi_{SC}$ that can be seen in Fig. 7(a), must be attributed to entropic effects, i.e., there are small changes in the packing or the average tilt of the lipid tails adjacent to the inclusion. The dependence of the hydrophobic mismatch at $\tau_{\min}$, $\Delta d_{\min}$, on the adsorption energy is presented in Fig. 7(b). It is of interest to mention that $\Delta d_{\min}$ increases more than linear with $\chi_{SC}$ especially for $\chi_{SC}>0$. This exemplifies the nontrivial variations in the lipid distribution around the inclusion.

### B. Radius of the inclusion

Here we will address the effect of the radius of the cylindrical object on the surface tension profile of the lipid bilayer as well as on the free energy of insertion. First we will present the membrane tension $\gamma$ as a function of distance from the inclusion. It is found that in the elastic region, i.e., for distances from the inclusion larger than $d_\ell^0$, the results can be fitted by the equation

$$\gamma(\Delta r) = A \exp\left(-\frac{\Delta r}{\xi}\right)\sin\left(2\pi\frac{\Delta r - \delta}{\lambda}\right), \tag{7}$$

where $\Delta r = r - R$, i.e., the distance from the surface of the inclusion. This equation corresponds to a damped wave with decay length $\xi$ and wavelength $\lambda$. $A$ is the extrapolated maximum amplitude at the inclusion's surface. In the limit $\Delta r \to \infty$ the bilayer is unperturbed and tensionless, i.e., the surface tension $\gamma=0$. Near the inclusion $\gamma>0$ if the bilayer thickness and lipid tail density are reduced with respect to the unperturbed bilayer and $\gamma<0$ if the bilayer thickness and the lipid tail density are larger than the unperturbed bilayer. At this point there may be a concern that a nonzero local surface tension of the membrane is mechanically unstable. However, the local bending of the lipid monolayers balances the lateral tension gradients such that stability is indeed maintained.

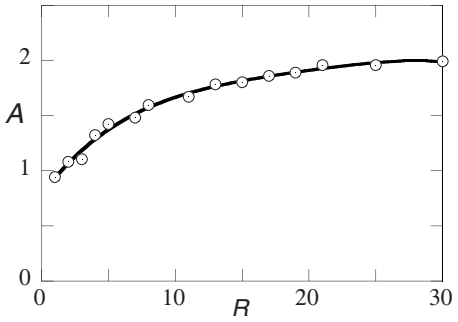


FIG. 8. The maximum amplitude A (in units $10^{-4}k_BT\ell^{-2}$) of the oscillations in the membrane tension as a function of the radius $R$ of the inclusion, for $\Delta d=0.86(t=8)$.

From our calculations it is found that both the wavelength $\lambda$ and the decay length $\xi$ do not depend on the radius of the inclusion $R$. These quantities are solely determined by the elastic properties of the bilayer. In addition, the offset of the oscillation $\delta$ does not depend much on $R$ either. The only parameter that shows a significant dependence on $R$ is the extrapolated maximum amplitude $A$ as is shown in Fig. 8. The results shown are for a hydrophobic mismatch $\Delta d=0.86$, i.e., for a tail length $t=8$, for which case the variation of $\gamma$ with $\Delta r$ is relatively large. The trends observed, however, are the same for other values of $\Delta d$. When the radius of the inclusion is increased, the amplitude $A$ goes to a limiting value for a flat surface. These results are in agreement with those of Lagüe *et al.* [28,29], who showed that the long-range oscillations become more pronounced when the inclusion's radius is increased.

Our calculations further show that the total insertion energy $\Omega$ depends almost linearly on $R$. This is easily explained since the interaction area between the inclusion and the bilayer is proportional to $R$. However, there is a small deviation from this linearity. This implies that there is a small curvature dependence of $\tau$, which again is related to small changes in the conformations of the lipids around the inclusion. It is possible to expand $\tau$ up to a second order Taylor series in the curvature $J_p(=1/R)$

$$\tau(J_p) = \tau_0 + \frac{\partial\tau}{\partial J_p}J_p + \frac{\partial^2\tau}{2\,\partial J_p^2}J_p^2 = \tau(0) - k_2J_0J_p + \frac{k_2}{2}J_p^2. \tag{8}$$

This equation defines the curvature modulus $k_2$ as the second derivative of $\tau(J_p)$ at $J_p=0$, and $J_0$ is the curvature where the line tension has an extreme (either a maximum or a minimum depending on the sign of $k_2$).

In Fig. 9 we present $[\tau(J_p)-\tau(0)]/J_p$ as a function of $J_p$ for several values of the hydrophobic mismatch $\Delta d$. The slope of the lines corresponds to $k_2/2$ and appears to be small and positive, i.e., in the range of 0.1 to 0.2. The intercept is given by $-J_0k_2$ and is negative showing that $J_0$ is positive and of order unity. From this it can again be concluded that $\tau$ does not depend strongly on $J_p$ and, in addition, that $\tau(0)$ is a reasonable measure for the normalized free energy of insertion even for low values of $R$. We will use this result below when we consider the interaction between two transmembrane objects in the bilayer.

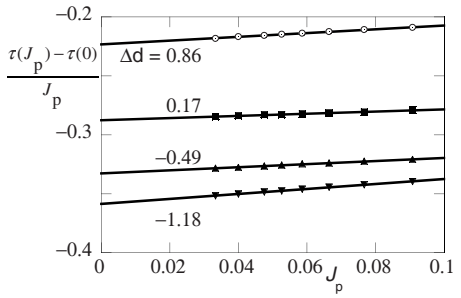


FIG. 9. The relation between $(\tau(J_p)-\tau(0))/J_p$ as a function of the curvature $J_p$ of the inclusion, with $\tau$ and $J_p$ in units $k_BT/\ell$ and $\ell^{-1}$, respectively. The slope gives information on the curvature modulus $k_2$.

### C. Lipid-mediated interaction between transmembrane objects

To obtain information on how objects in lipid bilayers interact with each other is a hard task. The analysis of the interaction between inclusions with radius $R$ in the bilayer generally calls for a three-gradient SCF analysis. For the time being this exceeds our computing facilities. For the limit of $R\to\infty$ however, the problem can be tackled with a two-gradient SCF analysis. The free energy of interaction in this case is given per unit length of the inclusion. Above we showed that the effects of the radius $R$ on the bilayer perturbations and the line tension are relatively small. For this reason we believe we can get useful information from such a two-gradient analysis of the lipid-mediated interaction between two inclusions. This is supported by studies in which the interaction between objects of different sizes has been investigated [36,42]. We will come back to this later in this section.

In studying the lipid-mediated interaction we will once again consider the effects of the hydrophobic mismatch $\Delta d$ and the contact interaction between the hydrophobic part of the inclusion and the lipid tails, characterized by $\chi_{SC}$.

The interaction free energy $F$ for a particular distance $H$ between the objects is plotted in Fig. 10 for two different cases, to which we will return below. In the literature various contributions of the free energy of interactions have been identified and discussed, ranging from several short-range contributions, such as depletion-induced interactions, lipid bridging, lipid packing, and less specified long range interactions [57]. We identify three different regimes, each having its own length scale in the interaction profile. First, there is the elastic interaction $F^e$, which results of the overlap of the inclusion-induced bilayer perturbations in the elastic region and which is dominant at distances $H>d_\ell^0$. In this regime the free energy of interaction $F(H)$ manifests itself as an exponentially decaying oscillation and can be fitted using an equation similar to Eqn (10). At the intermediate length scale, i.e., $2\sqrt{a_0}<H<d_\ell^0$, a second contribution becomes evident, namely a repulsive interaction $F^c$, which is in this $H$ range to a good approximation found by subtracting $F^e$ from $F$. In all cases we found that $F^c(H)$ decays approximately exponentially with $H$ as illustrated in Fig. 10. This interaction contribution is a consequence of the confinement of the lipid tails by the inclusions. For very small separations between the inclusions, i.e., $H<2\sqrt{a_0}$, the situation becomes more complex. We define the contribution $F^s(H)=F(H)-F^e(H)-F^c(H)$. The nature of this contribution strongly depends on the interaction of the tails with the surface of the inclusions. It can either reflect a depletion-induced attractive interaction [58] or a strongly oscillating and exponentially decaying interaction due to structural forces.

Two rather extreme cases of interaction profiles are shown in Fig. 10. Both graphs show $F$ as a function of $H$ and also the contributions $F^e$, $F^c$, and $F^s$ are depicted. Figure 10(a) is for the case that there is almost no hydrophobic mismatch, i.e., $\Delta d=-0.12$, and no effective lipid tail-inclusion interaction, i.e., $\chi_{SC}=\chi_{SV}$. It shows a repulsive barrier at intermediate separation and a depletion-induced attraction at short separation. A similar interaction profile has been found in several other studies on lipid-mediated interaction without mismatch and effective tail-inclusion interaction [22,28,36]. Figure 10(b) shows the case of a strong attractive tail-inclusion interaction, i.e., $\chi_{SC}=-1$, and a large positive mismatch, i.e., $\Delta d=0.86$. In this case strong oscillations in $F$ are present in the short-range regime. This situation has not been discussed before and it exemplifies the importance of the tail-inclusion interaction at short separations. Below, we discuss the findings for the three different length scales separately.

#### 1. Long-range interaction

On the longest length scale the lipid-mediated interaction is a consequence of the overlap of the structural bilayer perturbations. These perturbations result in a local variation in,

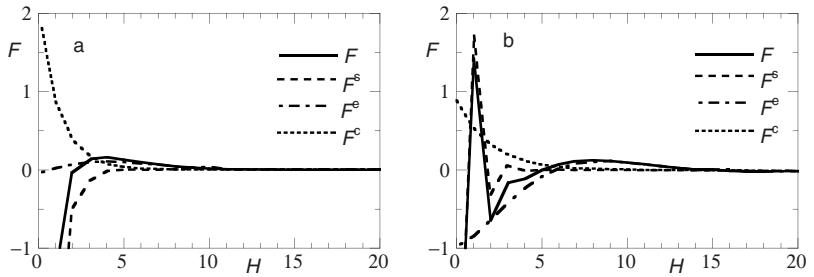


FIG. 10. The total interaction free energy $F$ (in units of $k_BT/\ell$) between two inclusions (with $R\to\infty$) as a function of their separation $H$. The interaction energy is the result of three contributions: a short-range segmental contribution $F^s$, an intermediate conformational contribution $F^c$ and a long-range elastic contribution $F^e$. (a) For the case of a small hydrophobic mismatch ($\Delta d=-0.12$) and no effective interaction between lipid tails and inclusion ($\chi_{SC}=\chi_{SV}$). (b) For a large mismatch ($\Delta d=0.86$) and attractive interaction ($\chi_{SC}=-1$).

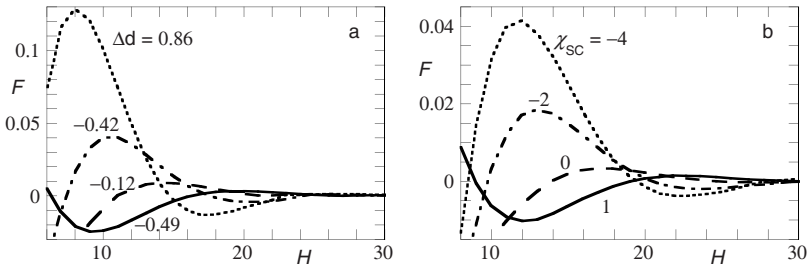


FIG. 11. The interaction energy $F$ (in units $k_BT/\ell$) between two rigid flat inclusions as a function of the separation between their surfaces $H$ (for $H>6$). (a) For several degrees of hydrophobic mismatch, i.e., several values of $\Delta d$ as indicated; $\chi_{SC}=-1$. (b) For various values of $\chi_{SC}$ ($t=12$ and $\Delta d=-0.12$}.

e.g., the bilayer thickness $d_\ell$, or the area per lipid molecule $a$, and have the same functional shape as the surface tension $\gamma(r)$ given in Eqn (10). As mentioned before, the wavelength $\lambda$ and the decay length $\xi$ of these perturbations are set by the structural and elastic properties of the bilayers. Figure 11 shows the energy of interaction for $H>d_\ell^0$, where $F^e(H) \approx F(H)$. As the force $f=-\partial F/\partial H$, the result shows that the interaction between the inclusions is attractive or repulsive depending on the distance $H$.

All the profiles shown in Fig. 11 can be fitted by

$$F(H) = A^F \exp\left(-\frac{H}{\xi^F}\right)\sin\left[2\pi\left(\frac{H-\delta^F}{\lambda^F}\right)\right]. \tag{9}$$

Here $\delta^F$ is the offset of the interaction profile and $\lambda^F$ its wavelength. The extrapolated maximum amplitude $A^F$ at $H=0$ shows the same dependence on $\Delta d$ and $\chi_{SC}$ as the amplitude $A$ in Eq. (10). For example, for $\chi_{SC}=-1$, both $A^F$ and $A$ show a minimum at $\Delta d \approx -0.65$. Furthermore, the wavelength $\lambda^F$ and decay length $\xi^F$ equal those that are found for the local surface tension variations expressed by Eq. (10). This indicates that they have the same origin. The oscillatory free energy curve may be rationalized using the elastic length scale concept [19,34]. Whether attraction or repulsion is found at some distance $H$ depends on the match or mismatch of integer number of elastic lengths between the surfaces. The elastic length is a characteristic bilayer property in the elasticity theory and it gives information on the decay of bilayer perturbations. It is defined as

$$\xi_e = \left[\frac{(d_\ell^0)^2 k_c}{k_a}\right]^{1/4} \tag{10}$$

with $k_c$ the bending modulus and $k_a$ the area compression-expansion modulus.

In Fig. 11(a) the variation of $F$ with the hydrophobic mismatch $\Delta d$ is shown. The hydrophobic mismatch determines the position of the first maximum and minimum in $F(H)$. The amplitude of the oscillation decreases exponentially with $H$ and there is a parabolic dependence on $\Delta d$. In Fig. 11(a) the largest maximum is found for $\Delta d=0.86$, amounting to approximately $0.12k_BT/\ell$. This implies that for $\ell=0.2-0.3$ nm this energetic barrier is large enough to amply overcome the thermal energy (approximately $1k_BT$), i.e., more than sufficient to prevent the inclusions from coming closer to each other, even for inclusions of a biologically relevant size. (This may be also the case for $\Delta d=0.42$). Compared to the first maxima in $F(H)$, the first elastic minima are relatively small. However, if such a minimum appears at relatively small $H$, it still may be deep enough to keep the inclusions at this distance from each other. This is for example the case for $\Delta d=-0.49$, where the minimum in interaction energy is about $-0.04k_BT/\ell$.

In Fig. 11(b) $F(H)$ is depicted for several values of $\chi_{SC}$ at a relatively small hydrophobic mismatch, i.e., $\Delta d=-0.12$. Just like $\Delta d$ the interaction parameter $\chi_{SC}$ affects the positions and heights or depths of the maxima and the minima in $F(H)$. For $\chi_{SC}=-4$ the height of the first elastic maximum is approximately $0.04k_BT/\ell$, which can in some cases be high enough to prevent inclusions from approaching each other closely. Thus even when the mismatch is small the elastic interaction can provide an effective energetic barrier. The first elastic minima in the studied cases are probably too small to accommodate the inclusions at this distance from each other.

In conclusion, the elastic maxima and minima in the interaction energy can be large enough to play a role in the organization of integral membrane structures in biological systems, even in the case of a relatively small hydrophobic mismatch. They may, for example, prevent the aggregation of membrane proteins and contribute to the ordering of membrane structures with (many) lipids between them.

#### *2. Intermediate-range interaction*

For intermediate distances, i.e., $2\sqrt{a_0} < H < d_\ell^0$, the interaction free energy $F$ cannot be described only by $F^e$. In this region another contribution must be taken into account, namely a repulsive interaction that decreases exponentially with $H$. This repulsion can be attributed to the loss of conformational entropy of the lipid tails as a consequence of the confined space between the two inclusions. It has also been discussed by May and Ben-Shaul [22], who used a simple director model as well as a molecular-level mean-field model. They showed that the interaction profile is not affected by constraints on the headgroup distribution. In some cases this repulsive contribution results in a barrier that is large enough to prevent the inclusions from approaching each other closely.

As mentioned above, to retrieve this intermediate-range interaction $F^c(H)$ we subtracted $F^e(H)$ from $F(H)$ in the intermediate distance range. The result can be fitted by

$$F^c(H) = A^c \exp(-H/\xi^c). \tag{11}$$

Here $A^c$ is the extrapolated amplitude at $H=0$ and $\xi^c$ the decay length. The decay length amounts to approximately two lattice sites. Within the accuracy of the determination of $\xi^c$ we did not find a dependency on the contact interaction $\chi_{SC}$ or on the tail length $t$.

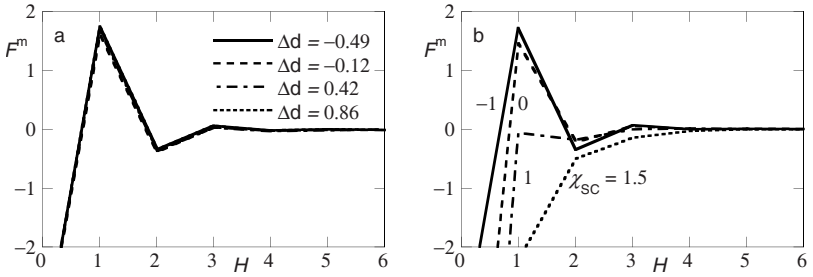


FIG. 12. The short-range interaction energy $F^s$ (in units $k_BT/\ell$). (a) For different values of $\Delta d$ with $\chi_{SC}=-1$. (b) For several values of $\chi_{SC}$ with $\Delta d=-0.12$.

### 3. Short-range interaction

In Fig. 12 the short-range interaction energy $F^s(H)$ is plotted. This interaction is defined as $F^s(H)=F(H)-F^e(H)-F^c(H)$ where the profiles of $F^e(H)$ and $F^c(H)$ have been extrapolated to $H=0$. Figure 12(a) shows that $F^s$ is not affected by the hydrophobic mismatch. In contrast, $\chi_{SC}$ has a strong effect on $F^s$.

The structural forces in this short range of interaction can lead either to attraction or to an oscillatory interaction, depending on the value of $\chi_{SC}$ [Fig. 12(b)]. A monotonic attractive structural force occurs if there is no affinity between the inclusion's surface and the lipid tails, equivalent to the depletion-induced attraction for a system of colloidal particles in a solution of nonadsorbing polymers as first described by Asakura and Oosawa [58]. This result was also obtained from Monte Carlo simulations [36]. If there is a strong affinity between lipid tails and inclusion, we observe a pronounced oscillatory interaction curve which decays rapidly with distance and results from the finite compressibility of the lipid core of the bilayer. Similar structural forces are seen for polymer melts confined between to solid surfaces. One of the consequences is that when the separation between the inclusions becomes small, a monomolecular lipid layer can stay in between them. Whether this will be the case depends entirely on $\chi_{SC}$. This means that the contact interaction not only determines whether a peptide or protein can be inserted in a lipid bilayer or not, but that it is also important to understand how proteins can pack densely in a lipid bilayer.

Due to computational reasons we have focused above on the interaction between two flat walls, mimicking large inclusions. This approximation is valid for distances $H$ between the inclusions that are small compared to the radius of the inclusions. To assess the implications of this approximation for separations comparable to $R$ and larger, we refer to the effects of $R$ on the perturbations caused by a single object in the bilayer membrane as described earlier in this paper. Our results show that $R$ primarily determines the amplitude of the oscillatory perturbation (in the membrane tension), which increases by about a factor of 2 going from very small $R$ to $R=30$ where a plateau is reached (see Fig. 8); $R$ does, however, not affect the wavelength or the decay length of the perturbation. These are set by the structural and elastic properties of the bilayer. In other words, increasing $R$ does not change the shape of the perturbation of the bilayer, only its intensity and this effect is limited and levels off. Therefore, we expect that using the simplification of two rigid walls overestimates the long-range elastic interactions between the inclusions less than an order of magnitude. In case the radius of the inclusions is small compared to the short and intermediate ranges of interaction defined here, one can assume that the inclusions have a square shape (from a top-view perspective), e.g., with (effective interaction) lengths $L$ for each side. One can then estimate the total free energy of interaction per inclusion with product $F(H)L$.

Another approximate route, which we here do not elaborate on, is to place a cylindrical inclusion with a fixed radius $R$ at the center of a Wigner-Seitz cell. The size of the cell is dictated by the average spacing between inclusions, and the central inclusion feels the surrounding ones by way of the reflecting boundary condition. This approach was used by Dan *et al.* [34]. Ideally, however one would like to solve the problem of many inclusions, floating in a bilayer, a typical three-gradient problem. It is not excluded that with increasing computational capabilities such problems may come into reach of SCF modeling in the near future.

From the above it follows that the free energy of interaction of inclusions is a nonmonotonic function of the distance between them. The interactions have been decomposed into various contributions and are linked to the perturbation of the structure of the membrane as a function of the distance away from the inclusion. Nonmonotonic interaction energies have been predicted on the basis of other models before and hence are well established. Direct comparison with previous predictions (see introduction) can only be done on a qualitative level because different authors use different models (using different normalizations) and include different contributions (for example the spontaneous curvature of the lipids and the shape of the inclusion [27,33,34]). The current analysis clearly confirms earlier findings that the elastic length, as given by Eq. (10), is important for understanding the interactions on a relatively large separation distance. In addition we showed that at intermediate length scales the perturbation of lipid conformations plays a role and finally the contact interactions of lipids with the inclusions are important as well. In this context, we address the question how realistic the model used is and, in particular, what that means for the interpretation of the results in terms of the interaction between real integral membrane biomolecules such as proteins. The crucial point is of course the assumption that transmembrane structures can be modeled as smooth rigid objects. As mentioned before, real proteins are flexible to some degree and have a more or less rough surface with different groups sticking out. We already indicated that therefore in the model the loss in conformational entropy of the lipid molecules near the inclusion is exaggerated, but this can be neutralized by using a large enough net attraction between the lipid tails and the surface of the inclusion, tunable through the interaction parameter $\chi_{SC}$. In addition, however, we expect that the

short-range oscillatory structural forces between inclusions are more pronounced in the model than in reality, since in the model at short interaction distances $H$ the lipids are confined between two flat and rigid walls. In contrast to this, in biological systems transmembrane structures are able to adjust their conformation to some extent in response to stress in the lipid bilayer.

Overall, we assess that the model gives good insight in the physical nature of the interactions between membrane-spanning inclusions in lipid bilayers and in the importance of factors like the elastic properties of the lipid bilayer, hydrophobic mismatch, and compatibility of lipid tails and the inclusion's surface.

## IV. CONCLUSIONS

We modeled the lipid bilayer structure around cylindrical membrane-spanning objects, mimicking structures such as transmembrane proteins and peptides, using a molecular level self-consistent field theory. In this paper we focused on the structural changes in the bilayer as a function of the affinity between the lipid tails and the inclusion and the effect of the inclusion's radius. Furthermore, the lipid-mediated interactions between two proteinlike inclusions were investigated.

The contact interaction with the lipid tail segments, characterized by the Flory-Huggins nearest-neighbor exchange parameter $\chi_{SC}$, determines to a large extent the total energy of inserting the object into the bilayer. Furthermore the packing of the lipid tails adjacent to the object and the degree of perturbation of the bilayer are affected by this interaction. As a consequence the energetically most favorable hydrophobic mismatch depends also on this short-range interaction. From this it follows that for transmembrane peptides and proteins in biological systems, accurate matching of the amino acid residues embedded in the hydrophobic core of the lipid bilayer as well as the length of the hydrophobic part of the transmembrane structure, is of crucial importance to avoid excessively large values of the insertion free energy.

The radius of the inclusion $R$ has only a minor effect on the density of the lipids directly adjacent to it. The presence of the transmembrane object leads to damped oscillations in the bilayer tension as a function of the distance from the object, of which the wavelength and decay length are not affected by $R$. Only the amplitude of the oscillations increases with the size of the object. Also the line tension of the bilayer around the inclusion is hardly affected by $R$.

The limited effect of the radius of the inclusion on the bilayer perturbations made it possible to simplify the modeling of the lipid-mediated interactions between two transmembrane objects to the case of $R \to \infty$. The results can be broken down into three contributions on distinct length scales. When the distance between the objects is larger than approximately the bilayer thickness, an exponentially decaying oscillating interaction profile is found, of which the wavelength and decay length correspond to the perturbations in membrane tension mentioned above and that strongly depends on the hydrophobic mismatch and tail-inclusion affinity. Depending on the specific parameters, this interaction can easily be strong enough to play a role in, e.g., the organization of proteins and peptides in biological membranes. At intermediate distances the conformational restriction of the lipid tails plays an important role resulting in a repulsive interaction. When the transmembrane objects approach each other closely, say closer than the average distance between the lipid molecules in the undisturbed bilayer, structural forces becomes important. If there is no strong attractive tail-inclusion interaction, a depletion-induced attraction between the transmembrane objects is found. Otherwise, an oscillating interaction is found which is due to the finite compressibility of the core of the lipid bilayer.

A basic assumption in this study is that transmembrane structures in biological membranes can be modeled like rigid cylindrical objects. We assess that this does not significantly affect the conclusions, although the short-range structural interactions as predicted by the model are probably much more pronounced than in reality. Despite the simplifications made, computational models as used here are valuable tools for gaining a better insight on the influence of membrane-spanning proteins and other molecules on the lipid bilayer structure and, ultimately, the organization of biological membranes.

[1] R. A. Kik, F. A. M. Leermakers, and J. M. Kleijn, Phys. Chem. Chem. Phys. **7**, 1996 (2005).
[2] A. Johannsson, C. A. Keightley, G. A. Smith, C. D. Richards, T. R. Hesketh, and J. C. Metcalfe, J. Biol. Chem. **256**, 1643 (1981).
[3] A. Johannsson, G. A. Smith, and J. C. Metcalfe, Biochim. Biophys. Acta **641**, 416 (1981).
[4] C. Montecucco, G. A. Smith, F. Dabbeni-Sala, A. Johannsson, Y. M. Galante, and R. Bisson, FEBS Lett. **144**, 145 (1982).
[5] J. R. Elliott, D. Needham, J. P. Dilger, and D. A. Haydon, Biochim. Biophys. Acta **735**, 95 (1983).
[6] M. Criado, H. Eibl, and F. J. Barrantes, J. Biol. Chem. **259**, 9188 (1984).
[7] R. J. Froud, C. R. A. Earl, J. M. East, and A. G. Lee, Biochim. Biophys. Acta **860**, 354 (1986).
[8] F. Michelangeli, E. A. Grimes, J. M. East, and A. G. Lee, Biochemistry **30**, 342 (1991).
[9] R. L. Cornea and D. D. Thomas, Biochemistry **33**, 2912 (1994).
[10] H. A. Rinia, R. A. Kik, R. A. Demel, M. M. E. Snel, J. A. Killian, J. P. J. M. van der Eerden, and B. de Kruijff, Biochemistry **39**, 5852 (2000).
[11] M. R. R. de Planque, E. Goormaghtigh, D. V. Greathouse, R. E. Koeppe II, J. A. W. Kruijtzer, R. N. J. Liskamp, B. de Kruijff, and J. A. Killian, Biochemistry **40**, 5000 (2001).
[12] T. Hessa, N. M. Meindl-Beinker, A. Bernsel, H. Kim, Y. Sato, M. Lerch-Bader, I. Nilsson, S. H. White, and G. von Heijne, Nature (London) **450**, 1026 (2007).

[13] S. H. White and G. von Heijne, Annu. Rev. Biophys. **37**, 23 (2008).
[14] M. M. Sperotto, S. May, and A. Baumgärtner, Chem. Phys. Lipids **141**, 2 (2006).
[15] W. Helfrich, Z. Naturforsch. **28C**, 693 (1973).
[16] H. W. Huang, Biophys. J. **50**, 1061 (1986).
[17] P. Helfrich and E. Jakobsson, Biophys. J. **57**, 1075 (1990).
[18] A. Ring, Biochim. Biophys. Acta **1278**, 147 (1996).
[19] C. Nielsen, M. Goulian, and O. S. Andersen, Biophys. J. **74**, 1966 (1998).
[20] P. Sens and S. A. Safran, Eur. Phys. J. E **1**, 237 (2000).
[21] C. Nielsen and O. S. Andersen, Biophys. J. **79**, 2583 (2000).
[22] S. May and A. Ben-Shaul, Phys. Chem. Chem. Phys. **2**, 4494 (2000).
[23] G. Brannigan and F. L. H. Brown, Biophys. J. **90**, 1501 (2006).
[24] G. Brannigan and F. L. H. Brown, Biophys. J. **92**, 864 (2007).
[25] D. R. Fattal and A. Ben-Shaul, Biophys. J. **65**, 1795 (1993).
[26] I. K. Valavanis, P. G. Bagosb, and I. Z. Emirisa, Comput. Biol. Chem. **30**, 416 (2006).
[27] N. Dan and S. A. Safran, Biophys. J. **75**, 1410 (1998).
[28] P. Lagüe, M. J. Zuckermann, and B. Roux, Biophys. J. **79**, 2867 (2000).
[29] P. Lagüe, M. J. Zuckermann, and B. Roux, Biophys. J. **81**, 276 (2001).
[30] U. Schmidt, G. Guigas, and M. Weiss, Phys. Rev. Lett. **101**, 128104 (2008).
[31] S. Marčelja, Biochim. Biophys. Acta **455**, 1 (1976).
[32] H. Schröder, J. Chem. Phys. **67**, 16 (1977).
[33] N. Dan, P. Pincus, and S. A. Safran, Langmuir **9**, 2768 (1993).
[34] N. Dan, A. Berman, P. Pincus, and S. A. Safran, J. Phys. II **4**, 1713 (1994).
[35] J.-M. Park and T. C. Lubensky, J. Phys. I **6**, 1217 (1996).
[36] T. Sintes and A. Baumgärtner, Biophys. J. **73**, 2251 (1997).
[37] K. S. Kim, J. Neu, and G. Oster, Biophys. J. **75**, 2274 (1998).
[38] P. Biscari and F. Bisi, Eur. Phys. J. E **7**, 381 (2002).
[39] K. Bohinc, V. Kralj-Iglič, and S. May, J. Chem. Phys. **119**, 7435 (2003).
[40] M. Goulian, R. Bruinsma, and P. Pincus, Europhys. Lett. **22**, 145 (1993).
[41] M. M. A. Claessens, F. A. M. Leermakers, F. A. Hoekstra, and M. A. Cohen Stuart, J. Phys. Chem. B **111**, 7127 (2007).
[42] Y. Lauw, F. A. M. Leermakers, and M. A. Cohen Stuart, J. Phys. Chem. B **111**, 8158 (2007).
[43] J. Sprakel, N. A. M. Besseling, M. A. Cohen Stuart, and F. A. M. Leermakers, Eur. Phys. J. E **25**, 163 (2008).
[44] L. A. Meijer, F. A. M. Leermakers, and J. Lyklema, J. Chem. Phys. **110**, 6560 (1999).
[45] F. A. M. Leermakers, A. L. Rabinovich, and N. K. Balabaev, Phys. Rev. E **67**, 011910 (2003).
[46] L. A. Meijer, F. A. M. Leermakers, and J. Lyklema, J. Phys. Chem. **99**, 17282 (1995).
[47] S. M. Oversteegen and F. A. M. Leermakers, Phys. Rev. E **62**, 8453 (2000).
[48] J. S. Rowlinson and B. Widom, *Molecular Theory of Capillarity* (Clarendon, Oxford, 1982).
[49] J. G. Kirkwood and F. P. Buff, J. Chem. Phys. **17**, 338 (1949).
[50] C. Tanford, *The Hydrophobic Effect: Formation of Micelles and Biological Membranes* (Wiley-Interscience, New York, 1980).
[51] H. T. Tien, J. Phys. Chem. **72**, 4512 (1968).
[52] D. W. R. Gruen and D. A. Haydon, Biophys. J. **30**, 129 (1980).
[53] E. A. DiMarzio and R. J. Rubin, J. Chem. Phys. **55**, 4318 (1971).
[54] R. J. Roe, J. Chem. Phys. **60**, 4192 (1974).
[55] T. K. M. Nyholm, S. Özdirekcan, and J. A. Killian, Biochemistry **46**, 1457 (2007).
[56] T. Hessa, H. Kim, K. Bihlmaier, C. Lundin, J. Boekel, H. Andersson, I. Nilsson, S. H. White, and G. von Heijne, Nature (London) **433**, 377 (2005).
[57] B. West, F. L. H. Brown, and F. Schmid, Biophys. J. **96**, 101 (2009).
[58] S. Asakura and F. Oosawa, J. Polym. Sci. **33**, 183 (1958).